Anomalous tracer diffusion in the presence of extended obstacles on a triangular lattice

I. Lončarević [a], D. Dujak [b], Z.M. Jakšić [c], A. Karač [d], Lj. Budinski-Petković [a],
S.B. Vrhovac [c,*]

[a] Faculty of Engineering, Trg D. Obradovića 6, Novi Sad 21000, Serbia
[b] Faculty of Metallurgy and Materials, University of Zenica, Bosnia and Herzegovina
[c] Scientific Computing Laboratory, Center for the Study of Complex Systems, Institute of Physics Belgrade, University of Belgrade, Pregrevica 118, Zemun 11080, Belgrade, Serbia
[d] Polytechnic Faculty, University of Zenica, Bosnia and Herzegovina

HIGHLIGHTS

- We study Lorentz gas on triangular lattice with extended scatterers (obstacles).
- Randomly placed non-overlapping obstacles are made by self-avoiding lattice steps.
- Obstacle shape becomes irrelevant for the singular behavior near the transition.
- Critical exponents do not depend on the size and shape of the obstacles.
- Non-Gaussian parameter grows with a power law in time at the percolation threshold.

ARTICLE INFO

ABSTRACT

Proteins diffuse to their sites of action within cells in a crowded, strongly interacting environment of nucleic acids and other macromolecules. An interesting question is how the highly crowded environment of biological cells affects the dynamic properties of passively diffusing particles. The Lorentz model is a generic model covering many of the aspects of transport in a heterogeneous environment. We investigate biologically relevant situations of immobile obstacles of various shapes and sizes. The Monte Carlo simulations for the diffusion of a tracer particle are carried out on a two-dimensional triangular lattice. Obstacles are represented by non-overlapping lattice shapes that are randomly placed on the lattice. Our simulation results indicate that the mean-square displacement displays anomalous transport for all obstacle shapes, which extends to infinite times at the corresponding percolation thresholds. In the vicinity of this critical density the diffusion coefficient vanishes according to a power law, with the same conductivity exponent for all obstacle shapes. At the fixed density of obstacles, we observe that the diffusion coefficient is higher for the smaller obstacles if the object size is defined as the highest projection of the object on one of the six directions on the triangular lattice. The dynamic exponent, which describes the anomalous transport at the critical density, is the same for all the obstacle shapes. Here we show that the values of critical exponents estimated for all disordered environments do not depend on the microscopic details of the present model, such as obstacle shape, and agree with the predicted values for the underlying percolation problem. We also provide the evidence

* Corresponding author.
  E-mail address: vrhovac@ipb.ac.rs (S.B. Vrhovac).
  URL: http://www.ipb.ac.rs/~vrhovac/ (S.B. Vrhovac).

for a divergent non-Gaussian parameter close to the percolation transition for all obstacle shapes.

1. Introduction

Particle transport in overcrowded environments, such as dense colloidal suspensions, supercooled liquids, lipid bilayers and cytoplasm, exhibit non-Gaussian behavior, dynamical heterogeneity, and anomalous diffusion [1–7]. Subdiffusion, for example, occurs if the mobility of a diffusing particle or molecule is impaired by obstacles or attractive forces. Then the trajectory of a particle tends to be trapped as time goes on, which can lead to deviation of the mean squared displacement (MSD) $\langle \Delta r^2(t) \rangle \propto t^\alpha$ from the linear Brownian scaling with time. The parameter α is the anomalous diffusion exponent which classifies the different types of diffusion: subdiffusion for $0 < \alpha < 1$, normal diffusion for $\alpha = 1$, and superdiffusion for $1 < \alpha \leq 2$; for $\alpha = 2$ the process is called ballistic [8,9].

There exist a number of stochastic models that describe the anomalous diffusion [7–13]. The analysis of such transport in disordered media by means of diffusion on percolation clusters was suggested by de Gennes [10]. The idea was to perform random walks on a percolation system. This can be used to measure the diffusion coefficient and to calculate the conductivity of the system via the Einstein relation for diffusion and conductivity [11]. Another class of models that is widely discussed is the fractional Brownian motion (FBM) [14] and the associated fractional Langevin equation motion [15]. FBM is based on superposition of the Brownian processes with a power-law memory. Subdiffusion in the FBM originates from an anticorrelation, which emerges in viscoelastic fluids [16]. The other model is a continuous time random walk (CTRW), which is a random walk with scale-free distributions of waiting times [17]. Anomalous transport can be generated within this framework by assuming that the mean trapping time diverges [8,12]. The last category, the Lorentz model, describes the transport in a spatially heterogeneous medium where the tracer explores the fractal-like structures that induce the anomalous dynamics [18]. This model consists of point particles that move freely until they encounter obstacles, often spheres, where they undergo elastic collisions. At high densities, the model exhibits a localization transition, i.e., above the critical density, a particle is always trapped by the obstacles. Direct link between the Lorentz model and the continuum percolation was also established [19–22].

One of the most characteristic features of the interiors of cells is the high total concentration of proteins, nucleic acids, and other biological macromolecules [23]. Under these conditions, the distance between neighboring proteins is comparable to their size. Diffusion of macromolecules is highly restricted by intermolecular steric repulsions as well as nonspecific attractive interactions. Such macromolecular crowding exerts large effects on the thermodynamic properties and kinetics of the processes, such as protein stability and enzyme activity [24,25]. Furthermore, molecule transport through the cell membranes, and protein interaction with specific DNA sequences constituting all of the biological functions of DNA are diffusion controlled processes. Proteins approaching their specific target sites on DNA and drugs on their way to their protein receptors are transported by diffusion [26]. It is interesting that active transport processes in living cells may lead to superdiffusion [27–31]. Therefore, diffusive processes in the cell play a central role in keeping the organism alive so that simulating the crowded intracellular environment is crucial for understanding the nature of living systems. In addition, the crowded systems include dense glassy systems of colloidal particles and hard spheres [32,33]. The dynamics of glass transition [32,33] was investigated for amorphous and granular materials [34,35] as well as for the supercooled liquids [36].

Particle diffusion in crowded environments has been in the focus of a number of computer simulations and theoretical studies [19,37–55]. Most of the previous studies have focused on studying transport through environments in which a single type of obstacle is present [19,37–46]. Due to relevance for the interpretation of single particle tracking experiments, percolation networks have been used to characterize the diffusive motion of tracer particles in crowded environments [45,46]. In particular, single trajectories of the tracer motion are analyzed to quantify the time averaged mean squared displacement (MSD) and to compare this with the ensemble averaged MSD of the particle motion. Since many biological environments contain multiple types of obstacles, simulation methods used to study the in vivo diffusion of macromolecules in crowded conditions should take into account obstacles of different shapes and sizes. Consequently, some previous studies have considered the effect of macromolecular shape on transport in the confined and crowded conditions typical for living biological cells [47–55].

In this paper we propose a lattice version of the Lorentz gas and use it to investigate the role that density and shape of the obstacles plays in the diffusion processes in crowded, heterogeneous environments. In the Lorentz lattice gas (LLG) [37,56] a tracer particle moves along the bonds of a lattice from lattice site to lattice site. When a particle arrives at a lattice site occupied by an obstacle, it encounters a scatterer that modifies its motion according to a given scattering rule. In our model, the environment heterogeneities are built by the obstacles of various shapes that are deposited at a randomly chosen site on the triangular lattice. Specifically, the obstacles are represented by self-avoiding lattice steps with sites that are considered forbidden for the point tracers. We try to deposit such obstacles with the beginning at the selected site in one of the six orientations chosen with an equal probability.

At low obstacle density, the tracer particle freely explores the lattice and exhibits normal diffusion. Above the critical obstacle density, the void space falls apart into a collection of finite-sized pores and tracer becomes confined in local pore space. In between, at short times the tracers do random walks in a fractal space and show the anomalous subdiffusion, but recover the normal diffusive behavior at long times. At the percolation threshold, the void space becomes a self-similar fractal in the statistical sense, and tracers show subdiffusion at all length and time scales. In the present model, the depositing objects (obstacles) are modeled by self-avoiding walks on the planar triangular lattice. We want to make a connection between the dynamics of a tracer and the percolation properties of extended obstacles on the lattice. In lattice models, the percolation threshold of randomly deposited non-overlapping objects depends on the coordination number of the lattice and on the size and shape of deposited objects. Therefore, three classes of objects (seven k-mers, two angled objects and two triangles) are selected with percolation thresholds in a wide range of values between 0.41 and 0.56 [57]. It must be stressed that in continuum percolation, the percolation threshold is quite high. For randomly placed non-overlapping disks the percolation threshold occurs at coverage fraction of 0.82, which is much higher than the density of obstacles in many biological environments [23].

In order to obtain a quantitative description of the dynamic properties over the full density range, the model parameters such as the obstacle size and thus coverage fraction of obstacles are systematically varied. We focus our attention on the influence of the shape of obstacles on the temporal behavior of the mean-square displacement, in particular for densities close to the percolation transition for given obstacles. We compare dynamics of a tracer in the presence of different obstacle shapes and discuss the scaling behavior of diffusion coefficients. In addition, we analyze the spatial heterogeneities in terms of the non-Gaussian parameter.

We organized the paper as follows. Section 2 describes the details of the model and simulations. The results of numerical simulations are presented in Section 3 which is divided into four parts. The first part of Section 3 contains the calculation of the percolation threshold for all obstacle shapes. In the second part we study the mean-square displacements for different obstacle shapes in a wide range of obstacle densities. Influence of the shape of obstacles on the density dependence of the diffusion coefficients is studied in the third part of Section 3. The fourth part is devoted to the analysis of the non-Gaussian parameter. Finally, Section 4 contains some additional comments and final remarks.

2. Definition of the model and the simulation method

The environment where tracer particles perform random walks is represented by the two-dimensional triangular lattice of size $L = 3200$. Periodic boundary conditions are used in all three directions of the lattice. They apply to the obstacles as well as to the paths of the tracer particles. In our model the lattice is initially occupied by immobile obstacles of various shapes and sizes at density θ_0. This density is defined as a fraction of sites of the lattice that are occupied by the obstacles. Linear obstacles are k-mers of length $\ell = k - 1 = 0, 1, \ldots, 5, 7$, shown in Table 1 as objects (A_1) – (A_5), (A_7). Extended shapes that we have used as obstacles are the crosses and triangles of two different sizes, shown in Table 2 as objects (B_2), (B_4), and (C_2), (C_5), respectively.

Obstacles cannot overlap and their spatial distribution at density θ_0 is generated using the random sequential adsorption (RSA) method [58,59]. In this way we are able to prepare K environments $\{C_i, i = 1, \ldots, K\}$ in disordered initial states with a statistically reproducible density θ_0 of obstacles. We always average our results over $K = 100$ such prepared disordered environments. After placing the obstacles up to the chosen density θ_0, we switch the obstacles deposition events off and initiate a random diffusive dynamics in the system. At this stage, the tracer performs a symmetric random walk, such that it is equally likely to find the tracer at any accessible site. Initially, tracer particle is randomly placed as a monomer on a vacant lattice site. Each site can be either empty or occupied by one particle: by a tracer particle or by a particle that belongs to an obstacle. A diffusion event starts by choosing one of the six possible directions at random, with equal probability, and try to move the tracer particle (monomer) by one lattice spacing in that direction. The particle is moved if it does not overlap with any of the previously deposited obstacles. The tracer particles have the same speed and their velocity directions are restricted to the six lattice vectors:

$$\boldsymbol{e_n} = \left(\cos\left(\frac{2\pi n}{6}\right), \sin\left(\frac{2\pi n}{6}\right) \right), \quad n = 0, 1, \ldots, 5. \tag{1}$$

It is convenient to set the speed of particles as well as the lattice constant both equal to 1.

In our model, a moving particle can never arrive at a lattice site occupied by an obstacle. When the particle move overlaps with any of the previously deposited obstacles, the particle movement is not performed and a new velocity direction is chosen. Its velocity direction changes according to stochastic rules. Here we assume isotropic scattering rules, i.e., postcollisional velocity directions have equal probabilities. We randomly pick one of them and search whether adjacent site in a randomly chosen direction is unoccupied. If so, we place the tracer particle. If the attempt fails, a new direction is selected at random. If necessary, we check all possible directions from the selected site in order to find a direction in which the tracer particle can be moved. In other words, no waiting time is allowed for tracer particle during the collision processes. Thus, the collision processes at obstacles are assumed to happen instantaneously or at least in negligible time. The time t is counted by the number of successful diffusion attempts. The simulations are carried out up to $t = 10^7$ successful diffusion attempts (in some cases, final time is increased up to $t = 10^8$).

3. Results and discussion

We have calculated the squared displacements for a tracer particle as running-time averages over at least $N = 1000$ independent trajectories for each realization of the obstacle disorder $\{C_i, i = 1, \ldots, K\}$ for a fixed density θ_0:

$$\Delta r^2(i; t) = \frac{1}{N} \sum_{j=1}^{N} |\mathbf{r}_j(i; 0) - \mathbf{r}_j(i; t)|^2, \quad i = 1, \ldots, K, \tag{2}$$

where $\mathbf{r}_j(i; t)$ is the position of the tracer particle at time t. The mean-square displacement (MSD) is given by

$$\langle \Delta r^2(t) \rangle = \frac{1}{K} \sum_{i=1}^{K} \Delta r^2(i; t). \tag{3}$$

The angular brackets $\langle \cdot \rangle$ here and in the following indicate the averaging both over the simulation ensemble $\{C_i\}$ in which the coverage fraction θ_0 of the obstacles is fixed (different realizations of the disorder) as well as over all initial positions of a particle.

We have extracted the diffusion coefficient D from the Einstein formula:

$$D = \lim_{t \to \infty} \frac{\langle \Delta r^2(t) \rangle}{4t}. \tag{4}$$

An alternative route to evaluate D is to perform the fitting procedure by a straight line to $\langle \Delta r^2(t) \rangle$ in the linear regime. We have checked that both methods yield similar results within statistical errors.

3.1. The percolation threshold

It would be interesting to compare the results describing diffusion properties of our model with the percolation properties of non-overlapping obstacles on the lattice. In order to obtain the values of the percolation thresholds for the objects of interest, additional simulations were performed on a triangular lattices of various sizes ranging from $L = 40$ to $L = 3200$. The tree-based union/find algorithm implemented on a grid platform was used to determine the occurrence of a percolation cluster [60]. Values of the percolation thresholds θ_p^* for the infinitely large lattice are obtained using the usual finite-size scaling analysis of the percolation behavior on two-dimensional lattices [61]. In such systems one assumes that the effective percolation threshold θ_p (the mean value of the threshold measured for a finite lattice) approaches the asymptotic value $\theta_p \to \theta_p^*$ ($L \to \infty$) via the power law:

$$\theta_p - \theta_p^* \propto L^{-1/\nu}. \tag{5}$$

Here the constant ν is the critical exponent that governs the divergence of the correlation length as $\xi \propto |\theta_p - \theta_p^*|^{-\nu}$. It should be noticed that the universality class of random percolation in two dimensions is very well identified and the critical exponents are known exactly, namely, $\nu = 4/3$ [61]. In our study, the typical values of lattice size are $L = 40, 60, 80, 100, 200, 400, 800, 1600, 3200$. Another quantity of interest is the jamming limit θ_J which is reached when no more depositing objects can be placed in any position on the lattice. Details of these simulations are given elsewhere [62,63]. Values of the obtained percolation thresholds θ_p^* for various objects are given in Tables 1 and 2 together with the corresponding jamming coverages θ_J.

3.2. Mean-square displacement

We now turn our attention to analysis of the tracer diffusion in the presence of various obstacles from Tables 1 and 2. As representative results, in Fig. 1 we present the MSD of tracer particles for the case of 5-mers (A_4) as obstacles in a wide range of densities $0.10 \leq \theta_0 \leq 0.70$. The curves have been plotted in a log–log scale so that normal diffusion yields a line of slope 1, and subdiffusion yields a line of lower slope. At short times tracer particles do not feel the presence of obstacles and they move freely. At very low densities of obstacles $\theta_0 \lesssim 0.1$, the initial transient is followed by the usual diffusive linear dependence on t. However, for higher densities an intermediate region develops where the system is subdiffusive. As seen from Fig. 1, region of anomalous diffusion can extends over several decades of time, before eventually entering the diffusive regime. This region extends to larger and larger times upon approaching a percolation threshold $\theta_p^* \approx 0.43$ for the obstacle (A_4). Due to the fact that the dynamics of a tracer particle moving on a lattice is dictated by the geometric exclusion effects, the subdiffusion at intermediate times becomes more pronounced with increasing the density of obstacles. For lower densities, we observe that the MSD reaches a linear time-behavior (diffusive regime) within the length of the simulation. However, for densities near to the percolation threshold $\theta_0 \lesssim \theta_p^* \approx 0.43$, a sublinear time dependence of MSD extends to the limit of our simulations ($t = 10^7$). At higher densities $\theta_0 > \theta_p^* \approx 0.43$,
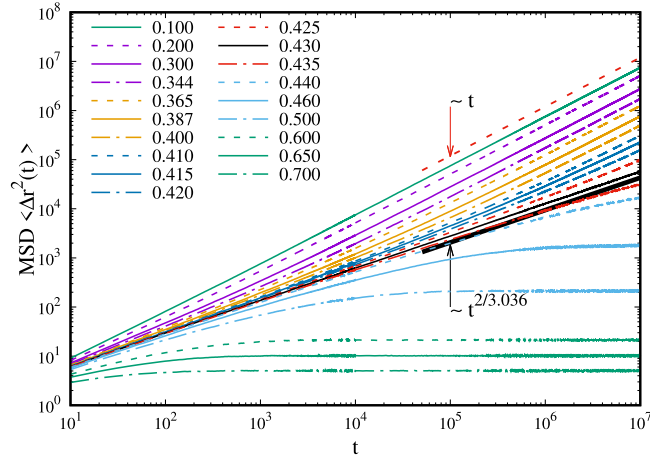
Fig. 1. Temporal evolution of the MSD $\langle \Delta r^2(t) \rangle$ for tracer particles in the presence of obstacles (A_4) (see, Table 1) at various densities θ_0. Obstacle density θ_0 increases from top to bottom $(\theta_0 = 0.1–0.7)$ as indicated in the legend. The solid straight line is the power-law (7) with exponent $2/z = 2/3.036$ (see, Eq. (10)).

normal diffusion is also absent, but the tracer particle is trapped in cages formed by the obstacles, and the mean-square displacement saturates. The phenomenon of localization is reflected in a plateau in the mean-square displacement, defining the localization length ℓ:

$$\langle \Delta r^2(t) \rangle = \ell^2 = \text{const.} \tag{6}$$

Numerical simulations for all obstacles shown in Tables 1 and 2 produce qualitatively similar results for the time dependence of the MSD in a wide range of the concentration θ_0 of obstacles.

As can be seen from Fig. 1, at the percolation threshold $\theta_0 = \theta_p^* \approx 0.43$ for the obstacle (A_4), the dynamics becomes neither diffusive nor trapped, and transport remains anomalous for all times. This feature can be directly inferred at the critical density θ_p^* for all other obstacles from the subdiffusive behavior of the mean-square displacement, which grows as

$$\langle \Delta r^2(t) \rangle \sim t^{2/z}, \quad z > 2, \tag{7}$$

for long times. Indeed, in Fig. 2 the results of the simulations for the MSD at the percolation threshold θ_p^* for obstacles (A_4), (B_4), and (C_5) are shown together with the fitting functions of the form (7). Our simulation results might indicate that the power law (7) is universal in the sense that it holds for any shapes of obstacles. Furthermore, dynamic exponent z is the same for all the obstacle shapes, $z = 3.036 \pm 0.034$. It must be emphasized that the dynamic exponent z is independent of the geometric exponents of the percolation problem. Its value is determined from the universality class of random resistor networks [61] (corresponding mathematical relation and estimated value are provided later in the text; see, Eq. (10)).

3.3. Diffusion coefficient

Dependence of the diffusion coefficient D_∞ on the density of obstacles θ_0 is shown in Figs. 3–6 for all examined objects (see, Tables 1 and 2). Here we have introduced the separation parameter ε which is defined as the normalized deviation of the density of obstacles θ_0 from the percolation threshold θ_p^*:

$$\varepsilon = \frac{\theta_p^* - \theta_0}{\theta_p^*}. \tag{8}$$

In Fig. 3 we compare the dependence of the diffusion coefficient D_∞ on the separation parameter ε for obstacles (A_0) – (A_5), and (A_7) (line segments of length $\ell = 0, 1, \ldots, 5, 7$). The double logarithmic plots of the diffusion coefficient D_∞ vs. separation parameter ε suggest a simple power-law dependence of D_∞ on ε for densities θ_0 close to the percolation thresholds θ_p^*:

$$D_\infty = A\, \varepsilon^\mu. \tag{9}$$

Solid lines through the data in Fig. 3 are the fits to Eq. (9). All fits have been performed for sufficiently high values of the obstacle density $\theta_0 \lesssim \theta_p^*$. We can see that these plots are mutually parallel straight lines for obstacles of very different
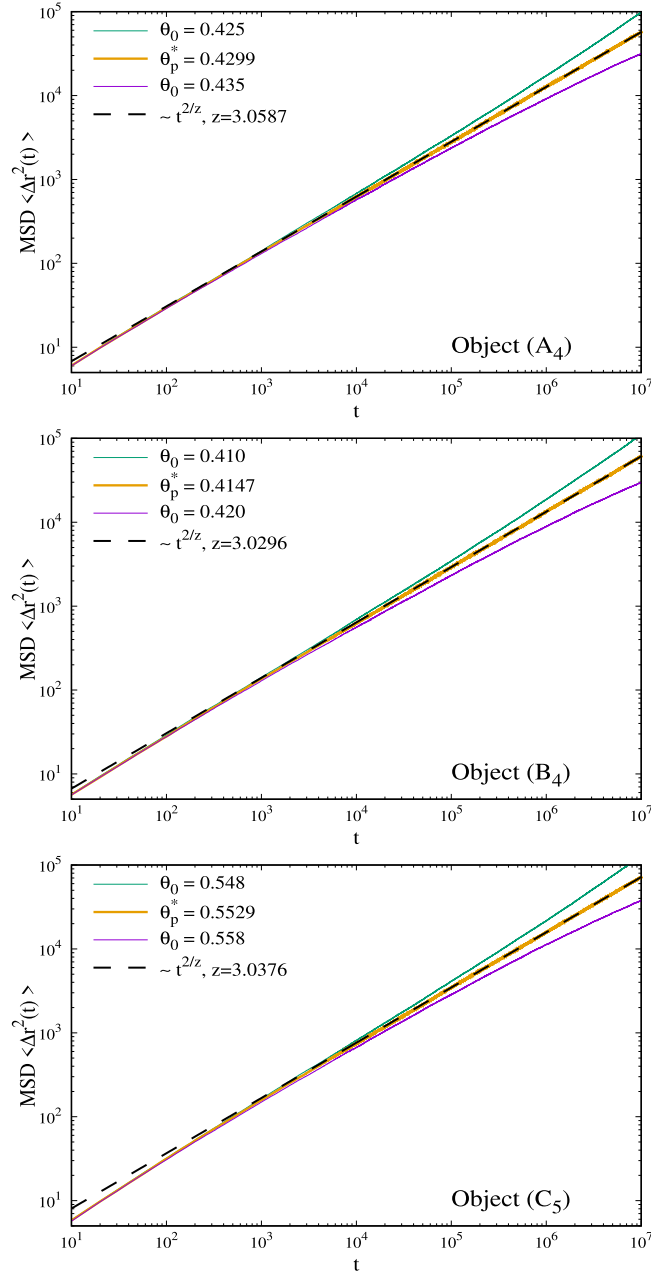
Fig. 2. Temporal evolution of the MSD $\left\langle \Delta r^2(t) \right\rangle$ for tracer particles in the presence of obstacles (A_4), (B_4), and (C_5) at the percolation threshold θ_p^* (see, Tables 1 and 2). The dashed superimposed lines are fits according to power law (7), with the exponents z given in the legends. The results for the MSD corresponding to the density of obstacles θ_0 just above and below the critical density θ_p^* are also shown for each object as indicated in the legends.

lengths. Consequently, as the percolation transition is approached, $\theta_0 \rightarrow \theta_p^*$, the diffusion coefficient D_∞ vanishes with a power law (9) that has the same exponent μ for all line segments (k-mers).

   We concentrate here on the influence of the shape of obstacles on the density dependence of the diffusion coefficients D_∞ for densities of obstacles below the percolation threshold θ_p^*. Fig. 4 shows the plots of D_∞ vs. ε for three obstacles, (A_2), (B_2), and (C_2), so that it contains results for various shapes of length $\ell = 2$ (see, Tables 1 and 2). The linear trends in Fig. 4 show the power law behavior as given by Eq. (9) in the range of densities θ_0 near the percolation thresholds θ_p^*, with the approximately equal exponent μ for all obstacles, (A_2), (B_2), and (C_2). As expected, the diffusion coefficient D_∞ is higher for smaller objects at a fixed density of obstacles θ_0. It should be noted that the object size s is taken as the greatest dimension of the object, i.e., as the greatest projection of the object on one of the six directions on the lattice.
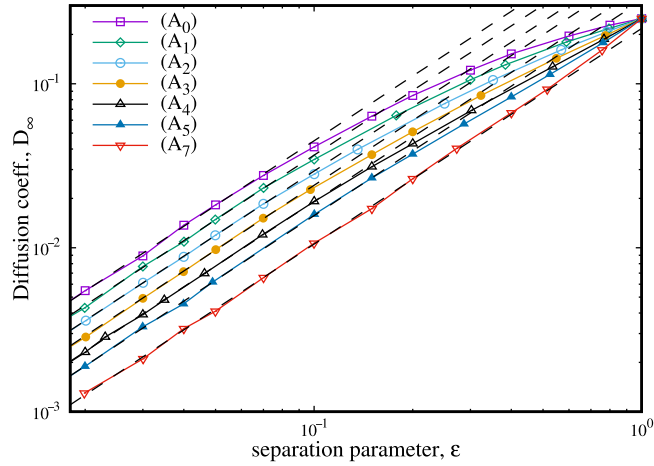
Fig. 3. Dependence of the diffusion coefficient D_∞ on the separation parameter ε (Eq. (8)) for obstacles (A_0)–(A_5), and (A_7) at densities below the percolation thresholds θ_p^* (see, Table 1). The dashed straight lines are the power-law fits, $D_\infty \propto \varepsilon^\mu$, for densities of obstacles θ_0 close to θ_p^*. For obstacles (A_0)–(A_5), and (A_7), values of fitting parameter are, respectively, $\mu = 1.3115, 1.3101, 1.3050, 1.3144, 1.3083, 13\ 117, 1.3156$.
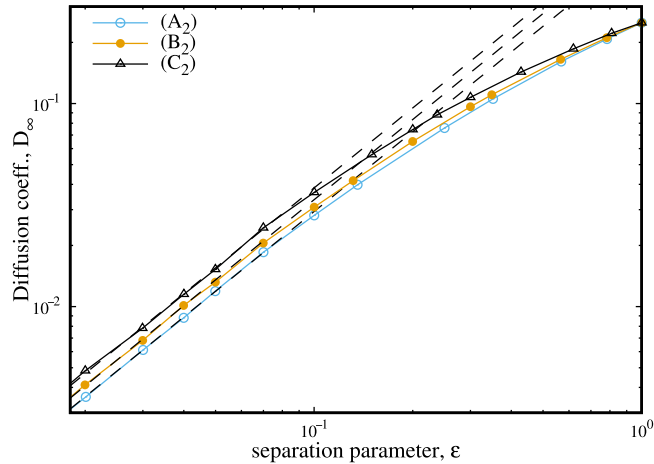
Fig. 4. Dependence of the diffusion coefficient D_∞ on the separation parameter ε (Eq. (8)) for obstacles (A_2), (B_2), and (C_2) at densities below the percolation thresholds θ_p^* (see, Tables 1 and 2). The dashed straight lines are the power-law fits, $D_\infty \propto \varepsilon^\mu$, for densities of obstacles θ_0 close to θ_p^*. For obstacles (A_2), (B_2), and (C_2), values of fitting parameter are, respectively, $\mu = 1.3050, 1.3116, 1.3075$.

Thus the size of a dot (A_0) is $s = 0$, the size of a one-step walk (A_1) is $s = 1$, and for example, the size of the first angled object (C_2) in Table 2 is $s = 1.5$ in lattice spacing. Here, we have $s(A_2) = 2$, $s(B_2) = 1.5$, and $s(C_2) = 1$, so that $D_\infty(A_2) < D_\infty(B_2) < D_\infty(C_2)$.

Qualitatively same results for the density behavior of the diffusion coefficient D_∞ are obtained for the extended obstacles of length $\ell = 4$ (Fig. 5) and $\ell = 5$ (Fig. 6). It must be stressed that the values of exponent μ in Eq. (9) for larger angled object (B_4) and triangle (C_5) do not differ from our estimates in the case of linear segments (A_0), (A_1), ..., or shapes (B_2) and (C_2). Consequently, for all obstacles we have obtained the confirmation of the power law (9) with the exponent equal to $\mu = 1.309 \pm 0.030$. The exponent μ nicely corroborates the value $\mu = 1.310 \pm 0.001$ which is obtained by Grassberger [64] in high-precision computer simulations for the electrical conductivity of a percolating lattice. By means of a scaling relation [61] connecting μ and z,

$$z = \frac{2\nu - \beta + \mu}{\nu - \beta/2}, \tag{10}$$

and using the reference value for the conductivity exponent $\mu = 1.310 \pm 0.001$ determined by finite-size scaling of the conductivity at the critical point [64], one finds the dynamic exponent $z = 3.036 \pm 0.001$, describing the anomalous transport at the critical density θ_p^* (see, Eq. (7)). Throughout this work, we use the universal lattice values for the geometric exponents $\nu = 4/3$ and $\beta = 5/36$ [61]. Measured value of the dynamic exponent $z = 3.036 \pm 0.034$ obtained in our numerical simulations is in excellent agreement with the value predicted by Eq. (10). Furthermore, the dynamic
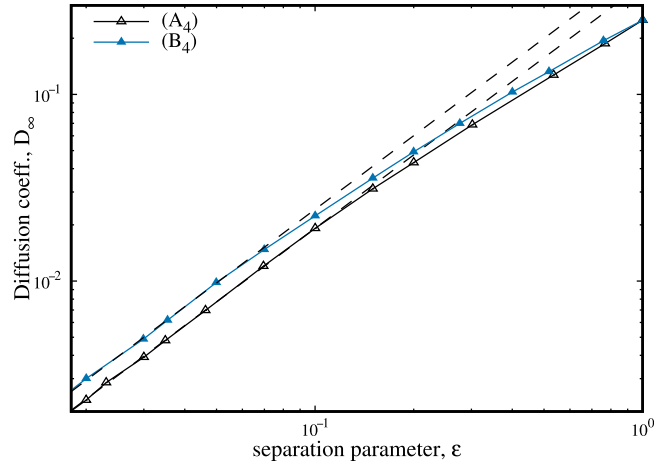
Fig. 5. Dependence of the diffusion coefficient D_∞ on the separation parameter ε (Eq. (8)) for obstacles (A_4) and (B_4) at densities below the percolation thresholds θ_p^* (see, Tables 1 and 2). The dashed straight lines are the power-law fits, $D_\infty \propto \varepsilon^\mu$, for densities of obstacles θ_0 close to θ_p^*. For obstacles (A_4) and (B_4), values of fitting parameter are, respectively, $\mu = 1.3083, 1.3108$.
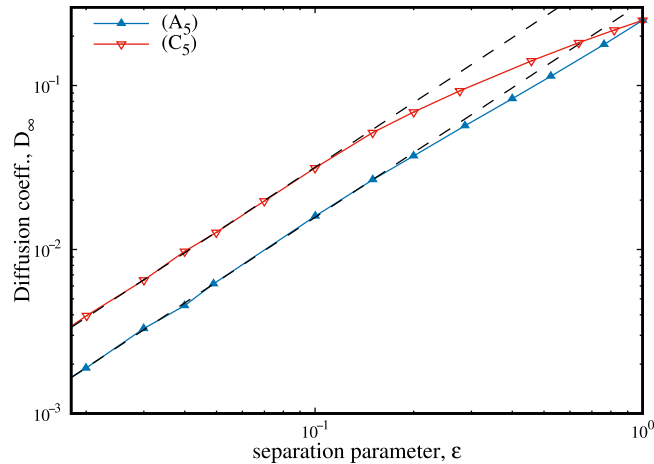

Fig. 6. Dependence of the diffusion coefficient D_∞ on the separation parameter ε (Eq. (8)) for obstacles (A_5) and (C_5) at densities below the percolation thresholds θ_p^* (see, Tables 1 and 2). The dashed straight lines are the power-law fits, $D_\infty \propto \varepsilon^\mu$, for densities of obstacles θ_0 close to θ_p^*. For obstacles (A_5) and (C_5), values of fitting parameter are, respectively, $\mu = 1.3117, 1.3114$.
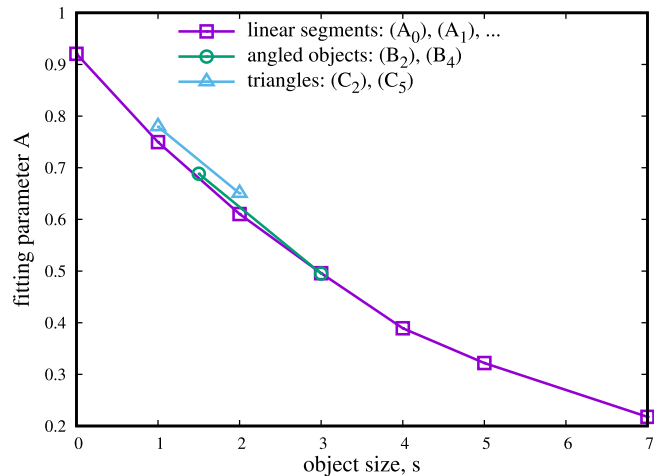
Fig. 7. Linear parameter A of fit (9) vs. object size s for all shapes in Tables 1 and 2.
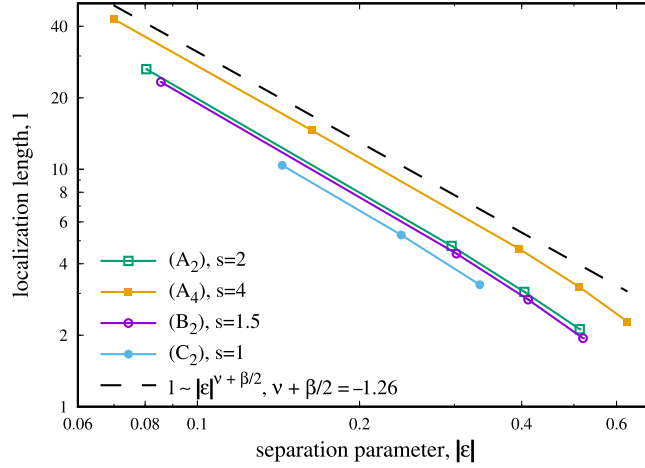
Fig. 8. Divergence of the localization length ℓ upon approaching the percolation threshold θ_p^* for obstacles (A_2), (A_4), (B_2), and (C_2) (see, Tables 1 and 2). The dashed straight line is the power-law (11) with exponent $-\nu + \beta/2 = -1.26$.

scaling analysis of anomalous transport due to the localization transition was performed for two-dimensional continuum models [21]. Extensive simulations for a Brownian tracer between overlapping circular obstacles confirmed the universal values of the dynamic exponents, e.g. for the exponent of subdiffusion $2/z \approx 0.659$ if also tracers in finite accessible clusters of all sizes are included.

In addition, the parameter A in Eq. (9) depends both on the shape and size s of the chosen obstacle. The fitting parameter A is less than 1 for all the obstacles considered and decreases with the object size s (see, Fig. 7).

At high densities, i.e., above a percolation threshold θ_p^*, the long-range transport ceases, $D_\infty = 0$, i.e. particle is always trapped by the obstacles (see, Fig. 1). The transition from diffusion to localization takes place during the percolation transition. As the density of obstacles is increased above a certain critical value θ_p^*, the initial large cluster of empty lattice space breaks into tiny separating components and connectivity between both sides of the lattice disappears. In other words, a geometric transition occurs at the percolation threshold θ_p^*, above which the void space falls completely apart into disconnected finite clusters. Consequently, tracers that are initially in a finite empty region on the lattice will remain there forever and do not contribute to the long-range transport. Percolation transition exhibits power law divergences of physical quantities with universal critical exponents. In particular, the localization length ℓ of the MSD (Eq. (6)) diverges with a power law upon approaching the critical density θ_p^* [19,21,61]:

$$\ell \propto |\varepsilon|^{-\nu+\beta/2}. \tag{11}$$

Moreover, ℓ can be calculated from the geometric exponents ν and β which are taken equal to their universal lattice values, $\nu = 4/3$ and $\beta = 5/36$ [61]. By calculating the exponent in Eq. (11), value $-\nu + \beta/2 = -1.26$ is obtained. Our simulations confirm that above the percolation threshold θ_p^*, the long-time limit ℓ^2 of the MSD is compatible with a power law (11) for various obstacle shapes (see, Fig. 8). As can be seen from Fig. 8, the curves $\ell(|\varepsilon|)$ shift to lower values when the object size s decreases.

### 3.4. Non-Gaussian parameter

In order to investigate the difference in the dynamics at lower densities of obstacles and that at higher densities, it is also convenient to introduce the non-Gaussian parameter (NGP) by

$$\alpha_2(t) = \frac{1}{2} \frac{\langle \Delta r^4(t) \rangle}{\langle \Delta r^2(t) \rangle^2} - 1, \tag{12}$$

where $\langle \Delta r^4(t) \rangle$ is the mean-quartic displacement (MQD) given by

$$\langle \Delta r^4(t) \rangle = \frac{1}{K} \sum_{i=1}^{K} \Delta r^4(i; t) = \frac{1}{K} \sum_{i=1}^{K} \frac{1}{N} \sum_{j=1}^{N} |\boldsymbol{r}_j(i; 0) - \boldsymbol{r}_j(i; t)|^4. \tag{13}$$

Again, the angular brackets $\langle \cdot \rangle$ indicate an averaging both over K realizations of the obstacle coverings with fixed density θ_0 as well as over N independent trajectories for each of K realizations of the obstacle disorder. For diffusion processes with a stationary Gaussian distribution of increments $\Delta \boldsymbol{r}(t) = \boldsymbol{r}(t) - \boldsymbol{r}(0)$, such as Brownian motion and fractional Brownian motion, the parameter $\alpha_2(t)$ should be strictly zero. However, this parameter deviates substantially from zero
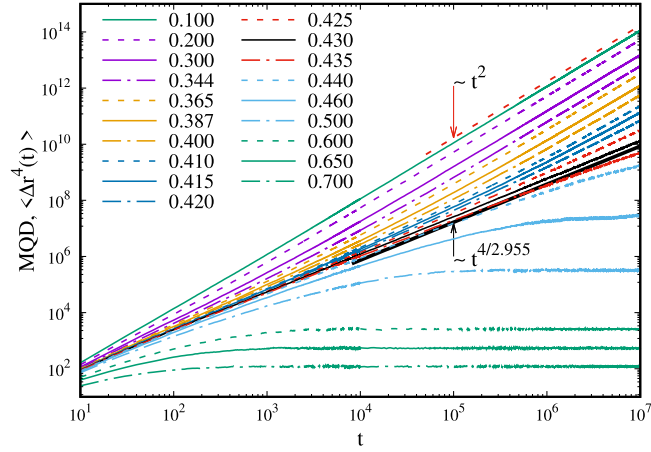
Fig. 9. Temporal evolution of the MQD $\left\langle \Delta r^4(t) \right\rangle$ for tracer particles in the presence of obstacles (A_4) (see, Table 1) at various densities θ_0. Obstacle density θ_0 increases from top to bottom ($\theta_0 = 0.1$–0.7) as indicated in the legend. The solid straight line is the power-law (14) with exponent $4/\tilde{z} = 4/2.955$ (see, Eq. (15)).
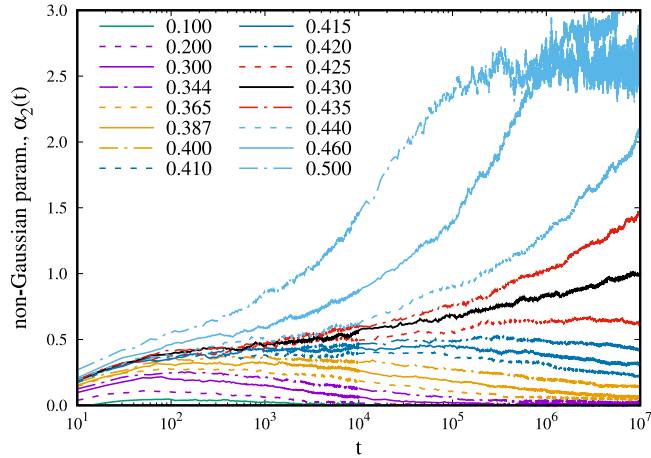
Fig. 10. Temporal evolution of the non-Gaussian parameter $\alpha_2(t)$ for tracer particles in the presence of obstacles (A_4) (see, Table 1) at various densities θ_0. Obstacle density θ_0 increases from top to bottom ($\theta_0 = 0.1$–0.5) as indicated in the legend.
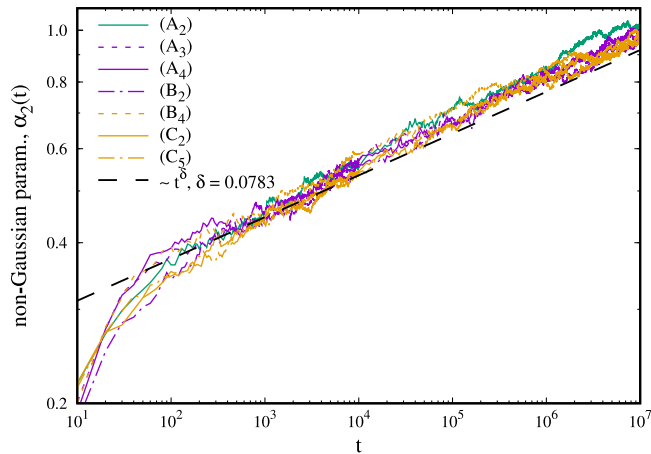
Fig. 11. Temporal evolution of the non-Gaussian parameter $\alpha_2(t)$ for tracer particles in the presence of obstacles (A_2), (A_3), (A_4), (B_2), (B_4), (C_2), and (C_5) at the percolation threshold θ_p^* (see, Tables 1 and 2). The dashed straight line is the power-law $\alpha_2(t) \sim t^\delta$ with exponent $\delta = 0.0783$.
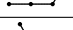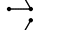
Table 1

Jamming coverages θ_J and the percolation thresholds θ_p^* for line segments (A_1), (A_2), (A_3), (A_4), (A_5), and (A_7) of different lengths $\ell^{(x)}$. Numbers in parentheses are the numerical values of the standard uncertainty of $\theta_J^{(x)}$ and θ_p^* referred to the last digits of the quoted values.

Obstacles	(x)	$\ell^{(x)}$	θ_J	θ_p^*
•	(A_0)	0	1	0.5000(1)
•—•	(A_1)	1	0.914033(3)	0.4867(1)
•—•—•	(A_2)	2	0.836211(4)	0.4628(3)
•—•—•—•	(A_3)	3	0.789090(6)	0.4432(2)
•—•—•—•—•	(A_4)	4	0.758458(7)	0.4299(4)
•—•—•—•—•—•	(A_5)	5	0.737031(9)	0.4206(5)
•—•—•—•—•—•—•—•	(A_7)	7	0.708962(12)	0.4124(6)

Table 2

Jamming coverages θ_J and the percolation thresholds θ_p^* for angled objects (B_2), (B_4), and triangles (C_2), (C_5) of different lengths $\ell^{(x)}$. Numbers in parentheses are the numerical values of the standard uncertainty of $\theta_J^{(x)}$ and θ_p^* referred to the last digits of the quoted values.

Obstacles	(x)	$\ell^{(x)}$	θ_J	θ_p^*
⌐	(B_2)	2	0.834440(4)	0.4606(6)
⌐	(B_4)	4	0.717995(7)	0.4147(4)
△	(C_2)	2	0.796940(5)	0.5246(1)
△	(C_5)	5	0.721062(7)	0.5529(6)

for the processes with non-stationary increments and/or non-Gaussian distributions, such as diffusion processes revealing a transient anomalous diffusion behavior [7,65].

At first, we focus our interest on the temporal evolution of the mean-quartic displacement (MQD) $\langle \Delta r^4(t) \rangle$ for various densities of obstacles θ_0. As representative results, in Fig. 9 we present the MQD of tracer particles for the case of 5-mers (A_4) as obstacles in a wide range of densities $0.10 \leq \theta_0 \leq 0.70$. Qualitatively the same results are obtained for all obstacles shown in Tables 1 and 2. For densities below the percolation threshold θ_p^*, the MQD reach long-time asymptotes $\langle \Delta r^4(t) \rangle \sim t^2$ as expected for diffusive motion. At a percolation threshold θ_p^*, temporal evolution of the MQD follows a power law

$$\langle \Delta r^4(t) \rangle \sim t^{4/\tilde{z}}, \tag{14}$$

over more than four decades in time. The exponent $\tilde{z}$ is the same for all the obstacle shapes, $\tilde{z} = 2.953 \pm 0.028$. At criticality, dynamic scaling predicts a power-law divergence (14) of $\langle \Delta r^4(t) \rangle$ with the parameter [19,66]

$$\tilde{z} = \frac{2\nu - \beta + \mu}{\nu - \beta/4} \approx 2.955. \tag{15}$$

We find agreement of our data with the prediction of continuum percolation. Indeed, for all obstacles at the percolation thresholds θ_p^*, the MQD follows the power law (14) with the predicted exponent $\tilde{z}$ (Eq. (15)) for a time window of several decades.

In Fig. 10 we display the non-Gaussian parameter $\alpha_2(t)$ of tracer particles for the case of 5-mers (A_4) as obstacles (Table 1) in a wide range of densities $0.10 \leq \theta_0 \leq 0.50$. As can be seen at densities below $\theta_0 \approx 0.3$, parameter $\alpha_2(t)$ approaches zero for long times. The decay to zero of $\alpha_2(t)$ at the late times for very low densities suggests that the statistics of increments $\Delta \boldsymbol{r}$ becomes a Gaussian. Our simulation data provides evidence for a significant increase of $\alpha_2(t)$ as density approaches the percolation threshold $\theta_p^* \approx 0.43$. In particular, parameter $\alpha_2(t)$ saturates at finite values for densities $0.30 \lessapprox \theta_0 < \theta_p^*$. The long-time limit of α_2 seems to diverge upon approaching θ_p^*. The NGP does not vanish in the diffusive regime at densities θ_0 close to the transition $\theta_p^* \approx 0.43$ due to the presence of localized particles (particles trapped in finite clusters). Recently, ergodic properties of a random walker performing anomalous diffusion on an ensemble of realizations of percolation clusters have been investigated by extensive Monte Carlo simulations [45] for a wide range of percolation densities. It has been shown that, at any percolation density, individual long time averaged MSDs do not always behave like ensemble averaged MSD. There exists a fraction of the time-averaged MSDs which significantly deviate from the time-averaged MSD averaged over both all individual simulated trajectories and over an ensemble of percolation geometries. These confined trajectories correspond to the trajectories when the particles motion is restricted on finite clusters of size significantly smaller than the system size. However, particles moving on the infinite cluster at criticality, display the convergence to the ensemble averaged MSD on the single trajectory level [45,67]. If tracers on all clusters are included, as in our model, the dynamics is nonergodic since the time average over a single trajectory differs from an ensemble average.

At the critical density θ_p^*, the non-Gaussian parameter $\alpha_2(t)$ is predicted to grow with a power law [7,19,20]:

$$\alpha_2(t) \sim t^{4/\bar{z}-4/z} = t^{\beta/(2\nu-\beta+\mu)}. \tag{16}$$

Representative examples of the double-logarithmic plots of parameter $\alpha_2(t)$ are shown in Fig. 11 for tracer diffusion in the presence of obstacles (A_2), (A_3), (A_4), (B_2), (B_4), (C_2), and (C_5) at corresponding percolation thresholds θ_p^* (see, Tables 1 and 2). For the long times, it seems that these curves are straight lines. The same is valid for all tested obstacles. Consequently, at the percolation threshold $\theta_0 \approx \theta_p^*$, the parameter α_2 diverges with a power law $\alpha_2(t) \sim t^\delta$ that has the same exponent $\delta = 0.0783$ for all obstacle shapes. The predicted exponent in Eq. (16) is very small, $\beta/(2\nu - \beta + \mu) = 0.0361$, but compatible with our data.

4. Summary

We have performed extensive Monte Carlo simulations of the motion of a point tracer in a two dimensional disordered environment in which immobile obstacles are densely packed and heterogeneously distributed. In order to examine the influence of shape and obstacle size on the diffusion characteristics of the system, a systematic approach was made by examining a wide variety of object shapes on a triangular lattice. The shapes are made by self-avoiding lattice steps, and their spatial distribution is generated by random deposition. Random sequential deposition of obstacles leads to the formation of branched structures on the lattice which restrict the space accessible to the tracer. Anomalous transport arises from the stochastic motion of the tracer in such maze-like structures.

We have focused on the anomalous transport, characterized by the power-law increase of the mean-square displacement on time windows covering several orders of magnitude. For all the obstacles considered, the region of anomalous diffusion extends to larger and larger times upon approaching a corresponding percolation threshold. At the percolation threshold, the transport remains anomalous for all times. In the present lattice based model, the critical density of the localization transition is defined by the percolation threshold. At obstacle densities below the critical density, tracer particles are able to diffuse over long distances, while at obstacle densities above the critical density all particles are trapped in finite regions.

We have shown that the percolation transition of the deposited obstacles is responsible for the suppression of the diffusion coefficient. As the percolation transition is approached, the diffusion coefficient D_∞ vanishes according to power law (9), with the same exponent $\mu = 1.309 \pm 0.030$ for all obstacles. This observation is consistent with the value of conductivity exponent $\mu = 1.310 \pm 0.001$, determined in high-precision computer simulations for the electrical conductivity of a percolating lattice [64]. Further, at a fixed density of the obstacles, the diffusion coefficient D_∞ is higher for the smaller obstacles. Here the object size is defined as the highest projection of the object on one of the six directions on the triangular lattice.

For obstacle densities at the percolation threshold, the void space is self-similar and the dynamics of a tracer becomes subdiffusive for long times (see, Eq. (7)). The dynamic exponent z in Eq. (7) can be determined from the scaling relation (10) which connects z and the conductivity exponent μ with the geometric exponents ν and β of the percolation problem. This value coincides with the numerical estimate $z = 3.036 \pm 0.034$ obtained from the simulations for all obstacles. Also, the exponent z was estimated to $z = 3.036 \pm 0.001$ from studies of the conductivity of random resistor networks [64], random walkers on percolation lattices [68] and in the overlapping 2D Lorentz model [21,69]. The value was confirmed also for the overlapping 2D Lorentz model with ballistic tracers [70]. For obstacle densities above the critical one, the mean-square displacement is obtained to saturate at the mean-square cluster size ℓ^2. Our simulations confirm that the long-time limit ℓ^2 of the MSD is compatible with the power law (11) for all obstacle shapes.

The values of the dynamic exponent z as well as the exponents for the diffusion coefficient μ and the localization length $\nu - \beta/2$, estimated from our simulation data for the critical density, agree with the predicted values for the percolation transition. Values of the critical exponents do not depend on the size and shape of the obstacles. The microscopic details of the present model, such as obstacle shape, become irrelevant for the singular behavior near the transition, and in this sense, the critical exponents are universal numbers.

The non-Gaussianity parameter $\alpha_2(t)$ is a sensitive indicator of the type of effective stochastic process driving the tracer particle in a spatially heterogeneous media. We found that the non-Gaussian parameter for the tracer particles yields finite values in the long-time limit, and it substantially increases as the localization transition is approached. In other words, the long-time regime is still non-Gaussian at the length scale covered by the simulation. Therefore, the dynamics is heterogeneous on such observational scales. The origin of the observed dynamical heterogeneity might be due to the presence of big holes in the random configuration of obstacles, that would lead to a finite probability of jumps much longer than the average. Such events correspond to the flights of a tracer particle between two successive collisions with obstacles where the particle finds a long free path between the obstacles. Furthermore, parameter $\alpha_2(t)$ grows with a power law in time (Eq. (16)) for all obstacles at the percolation threshold; the numerically determined exponent of 0.0783 is the same for all obstacle shapes.

As mentioned in the Introduction, protein transport in cells is anomalous due to the macromolecular crowding. In his seminal works, Saxton [71] recognized the biophysical relevance of Lorentz model for protein transport in cellular membranes. This minimalist model implies that the positions of lipids and proteins are restricted to a two-dimensional lattice; tracer molecules perform a random walk between randomly distributed obstacles occupying a single lattice site

each. In our study, intricate geometry of intracellular structures is mimicked by random obstacles of given shape. One of the limitations of our work is that we only considered one type of obstacle in each simulation. It might be more realistic to consider simulations where the lattice is populated by mixture of obstacles of different shapes and sizes. Moreover, diffusion of tracer particles of various sizes and shapes in poly-disperse mixtures of crowders, should be investigated.

Acknowledgments

References

[1] E.R. Weeks, D. Weitz, Subdiffusion and the cage effect studied near the colloidal glass transition, Chem. Phys. 284 (2002) 361–367.
[2] W.K. Kegel, A. van Blaaderen, Direct observation of dynamical heterogeneities in colloidal hard-sphere suspensions, Science 287 (2000) 290–293.
[3] J. Szymanski, M. Weiss, Elucidating the origin of anomalous diffusion in crowded fluids, Phys. Rev. Lett. 103 (2009) 038102.
[4] I. Golding, E.C. Cox, Physical nature of bacterial cytoplasm, Phys. Rev. Lett. 96 (2006) 098102.
[5] S.C. Weber, A.J. Spakowitz, J.A. Theriot, Bacterial chromosomal loci move subdiffusively through a viscoelastic cytoplasm, Phys. Rev. Lett. 104 (2010) 238102.
[6] T. Akimoto, E. Yamamoto, K. Yasuoka, Y. Hirano, M. Yasui, Non-gaussian fluctuations resulting from power-law trapping in a lipid bilayer, Phys. Rev. Lett. 107 (2011) 178103.
[7] F. Höfling, T. Franosch, Anomalous transport in the crowded world of biological cells, Rep. Progr. Phys. 76 (2013) 046602.
[8] R. Metzler, J. Klafter, The random walk's guide to anomalous diffusion: a fractional dynamics approach, Phys. Rep. 339 (2000) 1–77.
[9] R. Metzler, J. Klafter, The restaurant at the end of the random walk: recent developments in the description of anomalous transport by fractional dynamics, J. Phys. A: Math. Gen. 37 (2004) R161 – R208.
[10] P.-G. de Gennes, La Rech. 7 (1976) 919.
[11] S. Havlin, D. Ben-Avraham, Diffusion in disordered media, Adv. Phys. 51 (2002) 187–292.
[12] J.-P. Bouchaud, A. Georges, Anomalous diffusion in disordered media: Statistical mechanisms, models and physical applications, Phys. Rep. 195 (1990) 127–293.
[13] I.M. Sokolov, Models of anomalous diffusion in crowded environments, Soft Matter 8 (2012) 9043–9052.
[14] B. Mandelbrot, J. Van Ness, Fractional brownian motions, fractional noises and applications, SIAM Rev. 10 (1968) 422–437.
[15] E. Lutz, Fractional langevin equation, Phys. Rev. E 64 (2001) 051106.
[16] I. Goychuk, Viscoelastic subdiffusion: From anomalous to normal, Phys. Rev. E 80 (2009) 046125.
[17] H. Scher, E.W. Montroll, Anomalous transit-time dispersion in amorphous solids, Phys. Rev. B 12 (1975) 2455–2477.
[18] S. Havlind, D. Ben-Avraham, Diffusion in disordered media, Adv. Phys. 36 (1987) 695–798.
[19] F. Höfling, T. Franosch, E. Frey, Localization transition of the three-dimensional Lorentz model and continuum percolation, Phys. Rev. Lett. 96 (2006) 165901.
[20] F. Höfling, T. Munk, E. Frey, T. Franosch, Critical dynamics of ballistic and brownian particles in a heterogeneous environment, J. Chem. Phys. 128 (2008) 164517.
[21] T. Bauer, F. Höfling, T. Munk, E. Frey, T. Franosch, The localization transition of the two-dimensional Lorentz model, Eur. Phys. J. Spec. Top. 189 (2010) 103–118.
[22] M. Spanner, F. Höfling, G.E. Schröder-Turk, K. Mecke, T. Franosch, Anomalous transport of a tracer on percolating clusters, J. Phys.: Condens. Matter 23 (2011) 234120.
[23] K. Luby-Phelps, Cytoarchitecture and physical properties of cytoplasm: Volume, viscosity, diffusion, intracellular surface area, in: H. Walter, D.E. Brooks, P.A. Srere (Eds.), Microcompartmentation and Phase Separation in Cytoplasm, in: International Review of Cytology, vol. 192, Academic Press, 1999, pp. 189–221.
[24] R. Ellis, Macromolecular crowding: obvious but underappreciated, Trends Biochem. Sci. 26 (2001) 597–604.
[25] H.-X. Zhou, G. Rivas, A.P. Minton, Macromolecular crowding and confinement: Biochemical, biophysical, and potential physiological consequences, Ann. Rev. Biophys. 37 (2008) 375–397.
[26] M. Ptashne, A. Gann (Eds.), Genes and Signals, Cold Spring Harbor Laboratory Press, Cold Spring Harbor, New York, 2001.
[27] A. Caspi, R. Granek, M. Elbaum, Enhanced diffusion in active intracellular transport, Phys. Rev. Lett. 85 (2000) 5655–5658.
[28] N. Gal, D. Weihs, Experimental evidence of strong anomalous diffusion in living cells, Phys. Rev. E 81 (2010) 020903.
[29] J.F. Reverey, J.-H. Jeon, H. Bao, M. Leippe, R. Metzler, C. Selhuber-Unkel, Superdiffusion dominates intracellular particle motion in the supercrowded cytoplasm of pathogenic acanthamoeba castellanii, Sci. Rep. 5 (2015).
[30] I. Goychuk, V.O. Kharchenko, R. Metzler, How molecular motors work in the crowded environment of living cells: Coexistence and efficiency of normal and anomalous transport, PLoS One 9 (2014) 1–7.
[31] B. Tadić, S. Thurner, Information super-diffusion on structured networks, Physica A 332 (2004) 566–584.
[32] G.L. Hunter, E.R. Weeks, The physics of the colloidal glass transition, Rep. Progr. Phys. 75 (2012) 066501.
[33] F. Sciortino, P. Tartaglia, Glassy colloidal systems, Adv. Phys. 54 (2005) 471–524.
[34] L. Berthier, G. Biroli, Theoretical perspective on the glass transition and amorphous materials, Rev. Modern Phys. 83 (2011) 587–645.
[35] P.M. Reis, R.A. Ingale, M.D. Shattuck, Caging dynamics in a granular fluid, Phys. Rev. Lett. 98 (2007) 188301.
[36] P.G. Debenedetti, F.H. Stillinger, Supercooled liquids and the glass transition, Nature 410 (2001) 259–267.
[37] M. Saxton, Anomalous diffusion due to binding: a Monte Carlo study, Biophys. J. 70 (1996) 1250–1262.
[38] A. Godec, M. Bauer, R. Metzler, Collective dynamics effect transient subdiffusion of inert tracers in flexible gel networks, New J. Phys. 16 (2014) 092002.
[39] H. Berry, H. Chaté, Anomalous diffusion due to hindering by mobile obstacles undergoing Brownian motion or Orstein-Uhlenbeck processes, Phys. Rev. E 89 (2014) 022708.
[40] E. Vilaseca, A. Isvoran, S. Madurga, I. Pastor, J.L. Garcés, F. Mas, New insights into diffusion in 3d crowded media by monte carlo simulations: effect of size, mobility and spatial distribution of obstacles, Phys. Chem. Chem. Phys. 13 (2011) 7396–7407.

[41] S.K. Ghosh, A.G. Cherstvy, R. Metzler, Non-universal tracer diffusion in crowded media of non-inert obstacles, Phys. Chem. Chem. Phys. 17 (2015) 1847–1858.
[42] A. Wedemeier, H. Merlitz, C.-X. Wu, J. Langowski, How proteins squeeze through polymer networks: A cartesian lattice study, J. Chem. Phys. 131 (2009) 064905.
[43] S.K. Ghosh, A.G. Cherstvy, D.S. Grebenkov, R. Metzler, Anomalous, non-gaussian tracer diffusion in crowded two-dimensional environments, New J. Phys. 18 (2016) 013027.
[44] O. Bénichou, P. Illien, G. Oshanin, A. Sarracino, R. Voituriez, Tracer diffusion in crowded narrow channels, J. Phys.: Condens. Matter 30 (2018) 443001.
[45] Y. Mardoukhi, J.-H. Jeon, R. Metzler, Geometry controlled anomalous diffusion in random fractal geometries: looking beyond the infinite cluster, Phys. Chem. Chem. Phys. 17 (2015) 30134–30147.
[46] Y. Mardoukhi, J.-H. Jeon, A.V. Chechkin, R. Metzler, Fluctuations of random walks in critical random environments, Phys. Chem. Chem. Phys. 20 (2018) 20427–20438.
[47] F. Trovato, V. Tozzini, Diffusion within the cytoplasm: A mesoscale model of interacting macromolecules, Biophys. J. 107 (2014) 2579–2591.
[48] H.W. Cho, G. Kwon, B.J. Sung, A. Yethiraj, Effect of polydispersity on diffusion in random obstacle matrices, Phys. Rev. Lett. 109 (2012) 155901.
[49] T. Ando, J. Skolnick, Crowding and hydrodynamic interactions likely dominate in vivo macromolecular motion, Proc. Natl. Acad. Sci. 107 (2010) 18457–18462.
[50] S.R. McGuffee, A.H. Elcock, Diffusion, crowding & protein stability in a dynamic molecular model of the bacterial cytoplasm, PLoS Comput. Biol. 6 (2010) e1000694.
[51] M.J. Skaug, R. Faller, M.L. Longo, Correlating anomalous diffusion with lipid bilayer membrane structure using single molecule tracking and atomic force microscopy, J. Chem. Phys. 134 (2011) 215101.
[52] M. Cieśla, E. Gudowska-Nowak, F. Sagués, I.M. Sokolov, Tracer diffusion inside fibrinogen layers, J. Chem. Phys. 140 (2014) 044706.
[53] M. Cieśla, B. Dybiec, I. Sokolov, E. Gudowska-Nowak, Taming lévy flights in confined crowded geometries, J. Chem. Phys. 142 (2015) 164904.
[54] A.J. Ellery, R.E. Baker, S.W. McCue, M.J. Simpson, Modeling transport through an environment crowded by a mixture of obstacles of different shapes and sizes, Physica A 449 (2016) 74–84.
[55] J. Shin, A.G. Cherstvy, R. Metzler, Polymer looping is controlled by macromolecular crowding, spatial confinement, and chain stiffness, ACS Macro Lett. 4 (2015) 202–206.
[56] X.P. Kong, E.G.D. Cohen, Diffusion and propagation in triangular Lorentz lattice gas cellular automata, J. Stat. Phys. 62 (1991) 737–757.
[57] Lj. Budinski-Petković, I. Lončarević, M. Petković, Z.M. Jakšić, S.B. Vrhovac, Percolation in random sequential adsorption of extended objects on a triangular lattice, Phys. Rev. E 85 (2012) 061117.
[58] J.W. Evans, Random and cooperative sequential adsorption, Rev. Modern Phys. 65 (1993) 1281–1329.
[59] Lj. Budinski-Petković, I. Lončarević, D. Dujak, A. Karač, J.R. Šćepanovi, Z.M. Jakšić, S.B. Vrhovac, Particle morphology effects in random sequential adsorption, Phys. Rev. E 95 (2017) 022114.
[60] M.E.J. Newman, R.M. Ziff, Fast Monte Carlo algorithm for site or bond percolation, Phys. Rev. E 64 (2001) 016706.
[61] D. Staufer, A. Aharony, Introduction to Percolation Theory, Taylor & Francis, London, 1994.
[62] I. Lončarević, Lj. Budinski-Petković, S.B. Vrhovac, Simulation study of random sequential adsorption of mixtures on a triangular lattice, Eur. Phys. J. E 24 (2007) 19–26.
[63] Lj. Budinski-Petković, S.B. Vrhovac, I. Lončarević, Random sequential adsorption of polydisperse mixtures on discrete substrates, Phys. Rev. E 78 (2008) 061603.
[64] P. Grassberger, Conductivity exponent and backbone dimension in 2-d percolation, Physica A 262 (1999) 251–263.
[65] D. Ernst, J. Köhler, M. Weiss, Probing the type of anomalous diffusion with single-particle tracking, Phys. Chem. Chem. Phys. 16 (2014) 7686–7691.
[66] F. Höfling, T. Franosch, Crossover in the slow decay of dynamic correlations in the Lorentz model, Phys. Rev. Lett. 98 (2007) 140601.
[67] Y. Meroz, I.M. Sokolov, J. Klafter, Test for determining a subdiffusive model in ergodic systems from single trajectories, Phys. Rev. Lett. 110 (2013) 090601.
[68] A. Kammerer, F. Hfling, T. Franosch, Cluster-resolved dynamic scaling theory and universal corrections for transport on percolating systems, Europhys. Lett. 84 (2008) 66002.
[69] F. Höfling, K.-U. Bamberg, T. Franosch, Anomalous transport resolved in space and time by fluorescence correlation spectroscopy, Soft Matter 7 (2011) 1358–1363.
[70] M. Spanner, F. Höfling, S.C. Kapfer, K.R. Mecke, G.E. Schröder-Turk, T. Franosch, Splitting of the universality class of anomalous transport in crowded media, Phys. Rev. Lett. 116 (2016) 060601.
[71] M. Saxton, Anomalous diffusion due to obstacles: a monte carlo study, Biophys. J. 66 (1994) 394–401.